Accelerated Publications

Steady-State FTIR Spectra of the Photoreduction of Q_A and Q_B in *Rhodobacter sphaeroides* Reaction Centers Provide Evidence against the Presence of a Proposed Transient Electron Acceptor X between the Two Quinones

Jacques Breton*

Service de Bioénergétique, CEA-Saclay, 91191 Gif-sur-Yvette Cedex, France

Received February 12, 2007; Revised Manuscript Received March 5, 2007

ABSTRACT: In the reaction center (RC) of the photosynthetic bacterium *Rhodobacter sphaeroides*, two ubiquinone molecules, Q_A and Q_B, play a pivotal role in the conversion of light energy into chemical free energy by coupling electron transfer to proton uptake. In native RCs, the transfer of an electron from Q_A to Q_B takes place in the time range of 5−200 μs. On the basis of time-resolved FTIR step-scan measurements in native RCs, a new and unconventional mechanism has been proposed in which Q_B^- formation precedes Q_A^- oxidation [Remy, A., and Gerwert, K. (2003) *Nat. Struct. Biol. 10*, 637−644]. The IR signature of the proposed transient intermediary electron acceptor (denoted X) operating between Q_A and Q_B has been recently measured by the rapid-scan technique in the DN(L210) mutant RCs, in which the Q_A to Q_B electron transfer is slowed 8-fold compared to that in native RCs. This IR signature has been reported as a difference spectrum involving states X^+, X, Q_A, and Q_A^- [Hermes, S., et al. (2006) *Biochemistry 45*, 13741−13749]. Here, we report the steady-state FTIR difference spectra of the photoreduction of either Q_A or Q_B measured in both native and DN(L210) mutant RCs in the presence of potassium ferrocyanide. In these spectra, the CN stretching marker modes of ferrocyanide and ferricyanide allow the extent of the redox reactions to be quantitatively compared and are used for a precise normalization of the Q_A^-/Q_A and Q_B^-/Q_B difference spectra. The calculated $Q_A^-Q_B/Q_AQ_B^-$ double-difference spectrum in DN(L210) mutant RCs is closely equivalent to the reported $Q_A^-X^+/Q_AX$ spectrum in the rapid-scan measurement. We therefore conclude that species X^+ and X are spectrally indistinguishable from Q_B and Q_B^-, respectively. Further comparison of the $Q_A^-Q_B/Q_AQ_B^-$ double-difference spectra in native and DN(L210) RCs also allows the possibility that Q_B^- formation precedes Q_A^- reoxidation to be ruled out for native RCs.

The function of a number of biologically important energy-transducing membrane proteins such as cytochrome oxidase, cytochrome bc_1 or b_6f complexes, and photosynthetic reaction centers (RCs)[1] rests on the coupling between electron and proton transfer reactions. Because of the availability of structural data at ∼2 Å resolution, and because the electron transfer (ET) reactions can be initiated with a brief pulse of light, the RC of purple bacteria provides a paradigm for studying such reactions. In the RC of *Rhodobacter sphaeroides*, light excitation initiates fast transmembrane ET from the primary donor (P) to the primary quinone (Q_A) in ∼200 ps, and this is followed on a much slower time scale (∼100 μs) by the transfer of the electron to the secondary quinone (Q_B). Although quinones Q_A and Q_B are chemically identical molecules of ubiquinone-10, they play very different roles in the overall coupled electron and proton transfer reactions (for reviews, see refs *1* and *2*). Q_A is situated in a relatively hydrophobic environment, is tightly bound to the M subunit of the RC, and functions as a one-electron acceptor. In contrast, Q_B is situated in a more polar environment and is only tightly bound to the L subunit in its semiquinone (Q_B^-) state, the neutral quinone (Q_B) and doubly reduced quinol (Q_BH_2) being more loosely bound. Q_B undergoes conversion to the quinol in two successive reduction steps that are coupled to the uptake of two protons from the cytoplasm. These protons are delivered through a pathway formed by polar amino acid side chains and water molecules. The quinol is then released from the Q_B site for reoxidation in the cytochrome bc_1 complex, and the empty Q_B binding pocket is refilled by a quinone from the intramembrane quinone pool.

The two sequential ET reactions between Q_A and Q_B have been studied extensively by UV−vis and near-IR spectroscopy (*3*). It has been reported that the $Q_A^-Q_B \rightarrow Q_AQ_B^-$ reaction is biphasic with a fast phase (5−10 μs) that is

* To whom correspondence should be addressed: CEA-Saclay, Bât. 532, 91191 Gif-sur-Yvette Cedex, France. Phone: 331 69082239. Fax: 331 69088717. E-mail: cadara3@dsvidf.cea.fr.

[1] Abbreviations: RC, reaction center; IR, infrared; Q_A, primary quinone electron acceptor; Q_B, secondary quinone electron acceptor; P, primary electron donor; ET, electron transfer.

10.1021/bi700297b CCC: $37.00
Published on Web 03/24/2007

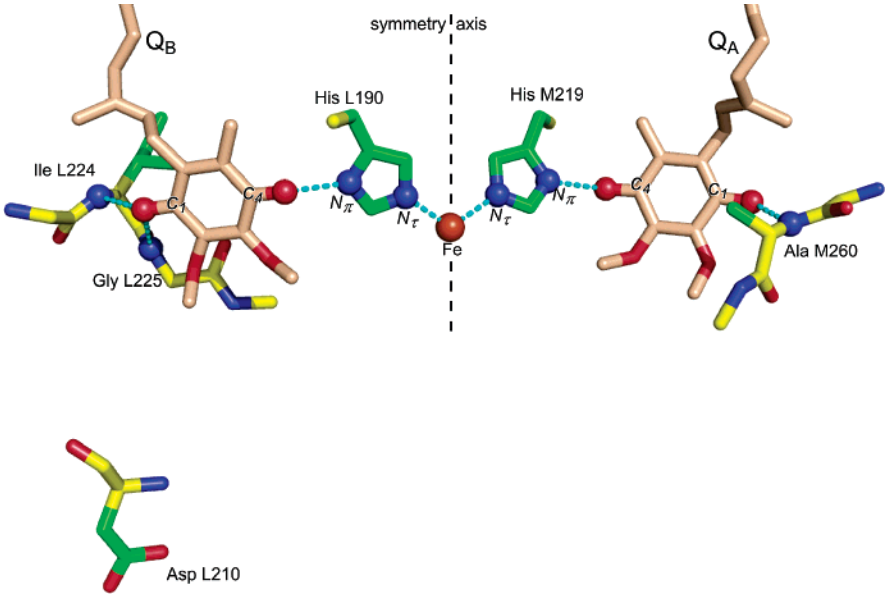

FIGURE 1: Interactions of Q_A and Q_B with the protein. The carbonyl groups of Q_A and Q_B engage in hydrogen bonds with the protein (cyan dots), and the two quinones are interconnected by a His−Fe−His bridge that straddles the axis of 2-fold symmetry (dashed line). Oxygen and nitrogen atoms are colored red and blue, respectively, with atoms engaged in bonding interactions shown as spheres. Carbon atoms are colored yellow for the protein backbone, green for side chains, and beige for the quinones. This figure, derived from PDB entry 2BOZ (*13*), has been kindly provided by M. Jones (University of Bristol, Bristol, U.K.).

assigned to pure ET and a slow phase (100−200 μs) for which the rate is independent of the driving force of the reaction (*4*, *5*). This slow phase appears to be kinetically gated by a conformational relaxation of the protein that occurs in response to reduction of Q_A. The precise nature of this relaxation is still unclear but is thought to involve conformational changes of the protein, charge relaxation, and/or protonation events (*5*, *6*). An approximately 5 Å movement and rotation of the Q_B quinone between two discrete binding sites, which has been proposed to be involved in the gating mechanism (*7*), appears to be a less likely candidate (*8*−*12*).

The X-ray structure of the bacterial RC shows Q_A and Q_B arranged in a near-symmetrical manner around an axis of approximate 2-fold symmetry that relates the L and M polypeptides (Figure 1). An iron atom sits on this symmetry axis between the two quinones and is connected to the C_4═O group of Q_A and Q_B via the side chains of His M219 and His L190, respectively. Investigations of the role of the His−Fe−His "bridge" between Q_A and Q_B have shown that the rate of the $Q_A^-Q_B \rightarrow Q_AQ_B^-$ reaction is essentially unchanged when the Fe^{2+} is replaced with other divalent metals (*14*) and is slowed by a factor of only 2 in Fe-depleted RCs (*14*).

Available X-ray crystal structures of the *Rb. sphaeroides* RC provide no information about the position of hydrogen atoms, such as those involved in hydrogen bonds to the quinone carbonyls for example, and are silent about the properties of most intermediates during the reaction cycle. However, complementary techniques such as EPR and ENDOR (*15*, *16*), as well as infrared (IR) spectroscopy, have been used to understand how the different properties of Q_A and Q_B can be explained by specific interactions with their protein environments. Notably, FTIR difference spectroscopy of the photoreduction of Q_A and Q_B (*17*−*26*) has been instrumental in establishing the hydrogen bonding state of the carbonyl groups of the quinones. The Q_A quinone shows a pronounced asymmetry in hydrogen bonding, with a remarkable downshift of the stretching frequency of its C_4═O carbonyl to 1601 cm^{-1}, indicating a very strong hydrogen bond with His M219 (*22*, *23*), and an unusually strong coupling of this 1601 cm^{-1} mode to a C═C mode absorbing at 1628 cm^{-1}. The C_1═O carbonyl of Q_A is in a suitable position to interact with the backbone amide of Ala M260, but this interaction does not result in a shift of the stretching frequency of this carbonyl group compared to that in solution. In contrast, the two carbonyl groups of Q_B engage in approximately equivalent moderate-strength hydrogen bonds with the surrounding protein. The stretching frequency of both Q_B carbonyl groups is located at 1641 cm^{-1}, downshifted by 10−20 cm^{-1} from their frequency in aprotic solvent (*24*, *25*). These results are consistent with X-ray structures of the RC that suggest that the C_4═O group of Q_B is hydrogen-bonded to His L190, while the C_1═O group is hydrogen-bonded to the backbone amide groups of Ile L224 and Gly L225 (Figure 1).

The pronounced spectral differences observed between the vibrational bands of Q_A and Q_B, which are also observed for the bands of the respective semiquinones (*19*, *20*), make them attractive markers for probing the $Q_A^-Q_B \rightarrow Q_AQ_B^-$ ET reaction, and several IR and FTIR kinetic techniques have been applied in studying the photoreduction of the quinones in the *Rb. sphaeroides* RC. In particular, light-induced transient spectra in native RCs were investigated by rapid-scan FTIR difference spectroscopy, allowing the contributions of Q_A, Q_A^-, Q_B, and Q_B^- to be revealed for the first time as a $Q_A^-Q_B/Q_AQ_B^-$ double-difference spectrum[2] (*17*). This double-difference spectrum turned out to be very similar to that calculated from the Q_A^-/Q_A and Q_B^-/Q_B FTIR difference spectra that were subsequently obtained under steady-state conditions (*20*). Transient signals associated with

[2] In such spectra, the vibrations of the Q_A^- and Q_B states appear as positive bands while those of Q_A and Q_B^- are negative.

the $Q_A^-Q_B \rightarrow Q_AQ_B^-$ ET reaction were characterized using tunable IR laser diodes (*27*) and later by step-scan FTIR spectroscopy (*28*). In the latter case, the reported $Q_A^-Q_B/Q_AQ_B^-$ double-difference spectrum between transient spectra measured at 7 μs and at 4.2 ms agreed well with those previously reported for measurements on slower time scales (*17*, *20*).

In 2003, Remy and Gerwert proposed a new and unconventional mechanism for the $Q_A^-Q_B \rightarrow Q_AQ_B^-$ reaction on the basis of step-scan measurements with a high time resolution. They reported the surprising result that the oxidation of Q_A^- was delayed with respect to the appearance of Q_B^-, implying the presence of a transient intermediary electron acceptor (denoted X and X^+ in the reduced and oxidized states, respectively) in the ET process (*29*). Although the redox state of the non-heme iron remains the same (Fe^{2+}) in both the $Q_A^-Q_B$ and $Q_AQ_B^-$ states (*30*, *31*), the Fe atom and its two bridging His side chains were considered attractive candidates for the X intermediate (*29*). However, a subsequent time-resolved X-ray absorption study ruled out the possibility of a transient change in the oxidation state of the non-heme iron on the time scale of the $Q_A^-Q_B \rightarrow Q_AQ_B^-$ ET reaction (*32*).

Recently, the nature of intermediate X has been investigated by a combination of rapid-scan and step-scan FTIR measurements on a mutant RC in which the $Q_A^-Q_B \rightarrow Q_AQ_B^-$ reaction is slowed by a factor of 8 compared to that in native RCs (*33*). In this mutant, denoted DN(L210), the Asp L210 residue located close to Q_B (Figure 1) is replaced with Asn (*1*). Because of the slowed kinetics of ET in the mutant, a $Q_A^-X^+/Q_AX$ difference spectrum was obtained with a high signal-to-noise ratio (*33*). Surprisingly, this spectrum exhibited striking similarities with $Q_A^-Q_B/Q_AQ_B^-$ double-difference spectra previously reported for native RCs (*17*, *20*, *28*). However, some differences were noted in the amide I and II regions of the protein absorption where the steady-state spectra of the DN(L210) mutant are known to differ from those of native RCs for both Q_B^-/Q_B (*34*−*36*) and Q_A^-/Q_A (*36*; J. Breton, M. L. Paddock, M. Y. Okamura, and E. Nabedryk, unpublished observations). Furthermore, the $Q_A^-X^+/Q_AX$ difference spectrum was reported in the range of 1900−1000 cm^{-1}, whereas all previously reported $Q_A^-Q_B/Q_AQ_B^-$ difference spectra extend to only 1200 cm^{-1}, thus precluding a comparison in the important region of absorption of the $C_5{-}N_\sigma$ mode of His side chains around 1100 cm^{-1}. In this work, we have reexamined the conditions used to generate the Q_A^-/Q_A and Q_B^-/Q_B FTIR difference spectra of native and DN(L210) mutant RCs and have found a means of normalizing all the difference spectra. The $Q_A^-Q_B/Q_AQ_B^-$ double-difference spectra calculated for native and DN(L210) mutant RCs in the range of 1800−1000 cm^{-1} are then compared to the $Q_A^-X^+/Q_AX$ spectrum recently reported for DN(L210) mutant RCs (*33*).

MATERIALS AND METHODS

DN(L210) mutant RCs were a kind gift from M. Paddock and M. Okamura (University of California at San Diego, La Jolla, CA). The preparation of the RC samples for FTIR spectroscopy of quinone photoreduction has been described previously (*19*−*22*, *24*, *34*). Briefly, the same buffer [100 mM Tris-HCl (pH 8.0)] containing potassium ferrocyanide (100 mM) and sodium ascorbate (10 mM) was used for all the samples. For Q_A^-/Q_A spectra, stigmatellin (2 mM) was added and continuous illumination was provided with saturating light filtered by a RG715 (Schott) filter and a water filter for heat removal. For Q_B^-/Q_B spectra, the RCs were reconstituted with an ~10-fold excess of ubiquinone-6 and excited with a saturating single-turnover Nd:YAG laser flash at 530 nm. Measurements were performed at 290 K. The spectral resolution was 4 cm^{-1}.

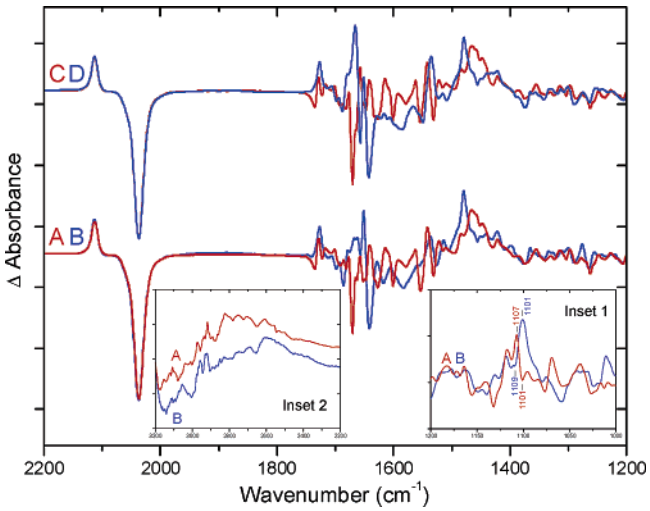

FIGURE 2: Light-induced steady-state Q_A^-/Q_A (A and C) and Q_B^-/Q_B (B and D) FTIR difference spectra for native RCs (A and B) and for DN(L210) mutant RCs (C and D). The spectra, measured under the same conditions of temperature, pH, and redox buffer, have been normalized on the CN stretching mode of ferricyanide and ferrocyanide responsible for the bands at 2113(+) and 2037(−) cm^{-1}, respectively. For native RCs, the spectra are depicted in the 1200−1000 and 3200−2200 cm^{-1} spectral range in insets 1 and 2, respectively. The resolution is 4 cm^{-1}. Tick marks are separated by 10^{-3} absorbance unit for trace A and by 2×10^{-4} absorbance unit in the insets.

RESULTS AND DISCUSSION

Normalized Q_A^-/Q_A and Q_B^-/Q_B FTIR Spectra of Native and DN(L210) Mutant RCs. The light-induced Q_A^-/Q_A and Q_B^-/Q_B FTIR difference spectra of native RCs in the 2200−1200 cm^{-1} spectral range are depicted in traces A and B of Figure 2, respectively. Those for the DN(L210) mutant RCs are shown in traces C and D, respectively. For each type of RC, the two spectra differ only in the presence or absence of the Q_B inhibitor stigmatellin or of excess ubiquinone-6 (for Q_A^-/Q_A or Q_B^-/Q_B, respectively) and in the nature of the saturating excitation light (continuous illumination and single-turnover laser flash for Q_A^-/Q_A and Q_B^-/Q_B, respectively). The four spectra (Figure 2) were normalized on the CN stretching mode of ferricyanide and ferrocyanide responsible for the bands at 2113(+) and 2037(−) cm^{-1}, respectively. These marker bands result from the fast reduction of the photooxidized primary donor in each radical pair ($P^+Q_A^-$ or $P^+Q_B^-$) by a ferrocyanide ion, thus generating a ferricyanide ion, and they disappear upon recombination of the semiquinone with a ferricyanide ion. The amplitude of these bands precisely monitors the amount of semiquinone formed in each RC sample, and as a result, these bands represent valuable markers for normalizing the Q^-/Q FTIR difference spectra recorded with different samples or under different conditions. To the best of our knowledge, this is

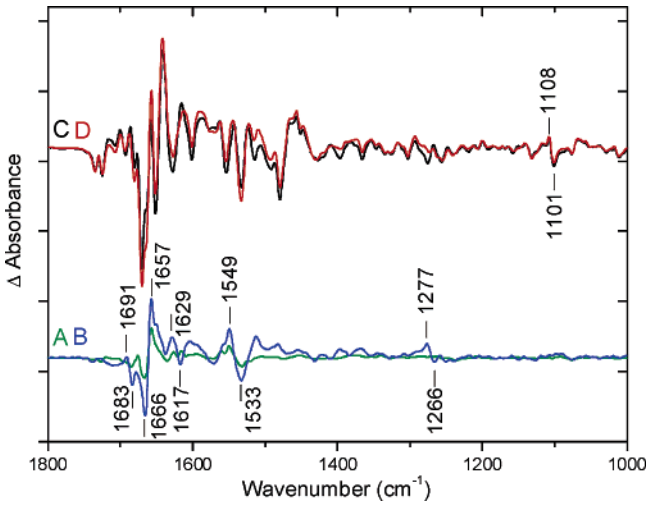

FIGURE 3: Double-difference spectra calculated from the steady-state Q_A^-/Q_A and Q_B^-/Q_B spectra depicted in Figure 2. Native-minus-DN(L210) mutant Q_A^-/Q_A (A) and Q_B^-/Q_B (B) double-difference spectra. $Q_A^-Q_B/Q_AQ_B^-$ double-difference spectra for native RCs (C) and for DN(L210) mutant RCs (D).

the first report of such normalization of difference spectra of this type. Previously, normalization of the difference spectra was performed on a more arbitrary basis by minimizing the residuals in the double-difference spectra (e.g., $^1H_2O - {}^2H_2O$ or native − mutant). The CN markers also offer an opportunity to determine the extinction coefficient of all the bands in the Q^-/Q FTIR difference spectra, taking into account the value of 1062 M^{-1} cm^{-1} for the ferricyanide band at 2113 cm^{-1} (*37*).

The Q_A^-/Q_A and Q_B^-/Q_B FTIR difference spectra of the native RC (traces A and B of Figure 2, respectively) were closely equivalent to those reported previously (*19*−*22*, *24*, *34*). The Q_B^-/Q_B FTIR difference spectrum of the DN(L210) mutant RC (Figure 2D) was also almost indistinguishable from those reported previously (*34*−*36*). The Q_A^-/Q_A spectrum of the DN(L210) mutant RC (Figure 2C) was similar to one previously reported (*36*), although the signal-to-noise ratio of the latter spectrum was rather low because of the rapid-scan conditions under which it was obtained. For native RCs, the Q_A^-/Q_A and Q_B^-/Q_B spectra are shown in the region of absorption of the $C_5{-}N_\sigma$ mode of His side chains around 1100 cm^{-1} (Inset 1) and in the spectral range of 3200−2200 cm^{-1} (Inset 2) corresponding to the broad continuum bands[3] previously assigned to excess protons in hydrogen bond networks (*38*). For the DN(L210) mutant RCs, the spectra in the latter two spectral windows (data not shown) are closely equivalent to those of native RCs.

Double-Difference Spectra of Native and DN(L210) Mutant RCs. Deviations of the Q_A^-/Q_A spectrum of the DN(L210) mutant RC (Figure 2C) from that of native RCs (Figure 2A) were quite small and mostly limited to the spectral range of absorption of the amide I and amide II modes around 1660 and 1540 cm^{-1}, respectively. These small deviations are best visualized in the native-minus-mutant double-difference spectrum (Figure 3A). Notably, they give rise to the two main differential features at ∼1666(−)/1657(+) and ∼1549(+)/1533(−) cm^{-1}. Interestingly, the corresponding double-difference spectrum for the Q_B^-/Q_B FTIR spectra for native and mutant RCs (Figure 3B) shows the two main differential features to be also located at the same position. These differential features correspond to the difference in the response of the protein backbone between native and DN(L210) mutant RCs upon semiquinone formation. The peptide C═O group of the L210 residue is situated closer to Q_B (distance of approximately 10 Å[4]) than to Q_A (approximately 24 Å) by a factor of ∼2.5. Surprisingly, the amplitude of the protein response upon Q_B reduction is only ∼2.5 times greater than that upon Q_A reduction. This effect is highly analogous to that previously reported for the electrostatic response to quinone reduction of vibrations of the bacteriopheophytin intermediary electron acceptor H_A located between P and Q_A (*39*). In this case, it was observed that upon Q_A reduction the electrostatic response of the 10a-ester C═O group of H_A was ∼2−3 times larger than when the negative charge was located on Q_B, despite the fact that the distance from that group to the center of the quinone rings[4] is roughly 2.5 times longer for Q_B than for Q_A (25 and 10.5 Å, respectively). The observation that the amplitude of the response of a protein or cofactor vibrational mode to the appearance of a negative charge on either one of the two quinones scales approximately linearly with the reciprocal of the distance provides strong evidence of a very high degree of electrostatic coupling between the Q_A and Q_B binding sites. This delocalized response of the whole medium to semiquinone formation must involve the many polar side chains and the network of ordered water molecules present in the vicinity of the Q_A and Q_B binding sites, as previously discussed (*38*−*40*; see also ref *2*).

Three additional small differential features centered around 1687, 1623, and 1271 cm^{-1} are resolved in the native-minus-mutant Q_B^-/Q_B double-difference spectrum (Figure 3B). The first two features most probably represent the response to Q_B reduction of the νC═O and δNH_2 vibrations of the Asn L210 side chain (*35*). The feature at 1271 cm^{-1} is likely to reflect a difference between native and mutant RCs for the geometry of the methoxy groups of Q_B, which are known to absorb in this frequency range (*21*, *24*).

Calculated $Q_A^-Q_B/Q_AQ_B^-$ double-difference spectra for the native and DN(L210) mutant RC are shown in traces C and D of Figure 3, respectively. These spectra are remarkably similar not only in terms of all the main features but also in terms of the frequency and amplitude of most of the small signals. The spectra are almost identical in the region of 1500−1430 cm^{-1} where the C⋯O and C⋯C modes of the Q_A^- and Q_B^- semiquinones contribute. The few main deviations between spectra C and D in Figure 3 are limited to the range of absorption of the amide I and amide II of the protein as well as in the region of absorption of the methoxy groups of Q_B (∼1270 cm^{-1}).

It should be noted that in the region of 1800−1200 cm^{-1} the $Q_A^-Q_B/Q_AQ_B^-$ double-difference spectra (traces C and D of Figure 3) exhibit many common bands with $Q_A^-Q_B/Q_AQ_B^-$ double-difference spectra previously reported for

[3] The shape of the continuum band in the Q_A^-/Q_A difference spectra was found not to depend upon the duration of the continuous illumination used during each cycle of measurement for illumination times ranging from 1 to 300 s.

[4] Distances (center-to-center) are from the center of the quinone ring of Q_A or Q_B to the oxygen of the peptide C═O group of Asp L120, or from the center of the quinone ring of Q_A or Q_B to the oxygen of the 10a-ester carbonyl of H_A. Data are taken from PDB entry 2BOZ (*13*).

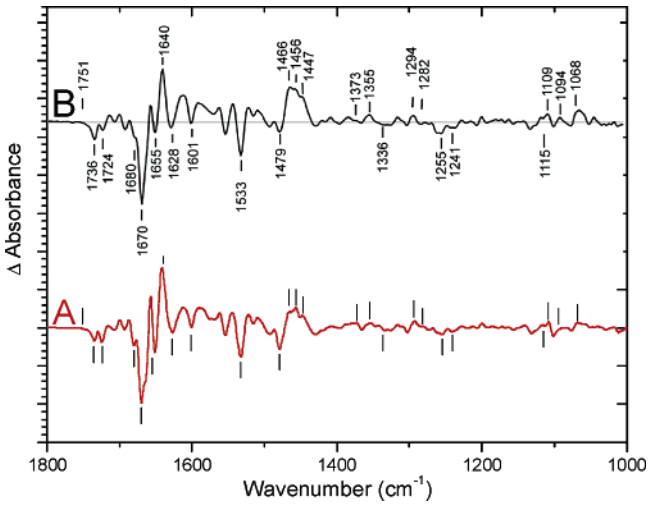

FIGURE 4: (A) $Q_A^-Q_B/Q_AQ_B^-$ double-difference spectra for DN(L210) mutant RCs (same spectrum as trace D of Figure 3). (B) $Q_A^-X^+/Q_AX$ spectrum recently reported from rapid-scan FTIR measurements on DN(L210) mutant RCs (*33*). The later spectrum, together with the original labels of the frequency of peaks, has been taken directly from the original PDF file in ref *33* and plotted on the same scale as trace A using Microsoft Powerpoint. The labels on spectrum A have been set at the same frequencies as those in spectrum B. Spectrum B was derived from measurements with the rapid-scan technique and was proposed to represent a $Q_A^-X^+/Q_AX$ FTIR difference spectrum (*33*).

native RCs using either the difference in the decay rates of the $P^+Q_B^-$ and $P^+Q_A^-$ states by a rapid-scan measurement (*17*), the static Q_A^-/Q_A and Q_B^-/Q_B FTIR spectra (*20*), or time-resolved $P^+Q_B^-$ and $P^+Q_A^-$ spectra obtained by the step-scan technique (*28*). Furthermore, the spectrum of a 1.1 ms phase in a step-scan measurement, assigned to the reduction of the oxidized intermediary acceptor X^+ by Q_A^- in native RCs (*29*), also has many features in common with the spectrum in Figure 3C.

Comparison of $Q_A^-X^+/Q_AX$ and $Q_A^-Q_B/Q_AQ_B^-$ Spectra of DN(L210) Mutant RCs. In Figure 4, the calculated $Q_A^-Q_B/Q_AQ_B^-$ double-difference spectrum of the DN(L210) mutant RCs (Figure 4A, same as Figure 3D) is compared with the $Q_A^-X^+/Q_AX$ difference spectrum (Figure 4B) recently reported from rapid-scan FTIR measurements on the same mutant (*33*). The latter spectrum, together with the original labels of the frequency of peaks, has been taken directly from the original PDF file in ref *33* and is plotted on the same scale as Figure 4A (an ASCII file of the spectrum in Figure 4A is available as Supporting Information). The matching of the positions and relative amplitudes not only of the major bands but also of the smallest details of the spectra is striking. Because of the ± 1 cm^{-1} precision of the frequency given for the bands, all of the labeled features in Figure 4B match closely those in Figure 4A with the only exception of the negative band at 1655 cm^{-1}, for which a 3 cm^{-1} shift in the peak position is observed. This frequency corresponds to the region of maximum absorption of the amide I C═O band, and of the intense scissoring mode of water.

The close equivalence of the two spectra depicted in Figure 4 provides compelling evidence that they involve chemical species having the same IR fingerprints. Importantly, this equivalence is also observed for the spectral features around 1100 cm^{-1} where the $C_5{-}N_\sigma$ mode of His side chains absorbs (*41*). It was essential to analyze this spectral region as one of the most likely candidates for a putative species X would be the His M219 and His L190 side chains bridging from the Fe^{2+} ion to the quinones. From the close equivalence of the two difference spectra depicted in Figure 4, we are therefore led to the conclusion that the contribution to the IR spectra of the species described as X^+ and X in (*33*) cannot be distinguished from those of Q_B and Q_B^-, respectively. The Q_A^-/Q_A and Q_B^-/Q_B FTIR difference spectra used to calculate the spectrum in Figure 4A correspond to fully relaxed species. Therefore, we cannot at present exclude the possibility that the very small differences with the spectrum in Figure 4B represent contributions from some form of unrelaxed Q_B^- in the rapid-scan measurements. Assessing this possibility would require further analysis of rapid-scan and steady-state measurements performed on the same samples and with the same instrument.

It is not the purpose of this work to discuss in detail the analysis of the kinetic data which led the authors of ref *33* to propose a new mechanism involving the role of X^+ and X as a transient redox intermediate between Q_A and Q_B. However, it should be noted that complementary rapid-scan and step-scan measurements on stigmatellin-inhibited RCs, where the $Q_A^-Q_B \rightarrow Q_AQ_B^-$ ET reaction is blocked, have not been reported. This control represents a key experiment for several reasons. First, the 9 ms kinetic phase derived from the analysis of the rapid-scan data (*33*) is close to the time resolution of the measurement. Second, for the experiments performed in the presence of the mediator 2,3,5,6-tetramethyl-*p*-phenylenediamine (DAD), it is important to determine the time evolution of the DAD^+/DAD redox couple as these species have IR absorption bands that overlap with those of the Q^-/Q species (J. Breton, unpublished observations). Finally, transient displacement of charges arising from electron and/or proton transfer reactions following Q_A reduction has been reported to occur in the time range of 100−200 μs in such Q_B-inhibited samples (*42*). The molecular events that accompany this relaxation following the formation of Q_A^- and which are likely to represent at least part of the gating mechanism for the $Q_A^-Q_B \rightarrow Q_AQ_B^-$ ET reaction are bound to lead to transient IR changes on the same time scale. Furthermore, one cannot exclude the possibility that relaxation dynamics around P^+ also occur on time scales commensurate with those determined in the kinetic FTIR measurements (*33*).

In conclusion, the analysis of the normalized Q_A^-/Q_A and Q_B^-/Q_B light-induced FTIR difference spectra of native and DN(L210) mutant RCs has provided strong evidence that the X^+/X redox pair previously proposed to act as a transient electron intermediate in the $Q_A^-Q_B \rightarrow Q_AQ_B^-$ ET reaction in both native and mutant RCs (*29*, *33*) exhibits all the IR fingerprint signatures of the Q_B/Q_B^- couple. In addition, the data provide semiquantitative information about the importance of the electrostatic cross talk between the environment of the Q_A and Q_B binding sites. Finally, the transient protonation of Asp L210 discussed in ref *33*, which was partly based on rapid-scan and step-scan FTIR measurements performed at 1751 cm^{-1} where a large contribution from 10a-ester C═O vibration(s) of P^+ dominates the absorption changes (*17*), should probably be reconsidered in view of these results. However, the idea of protonation of water in a

continuum of hydrogen bonds in the vicinity of Q_B^-, as originally discussed in ref *38*, remains of interest and deserves further investigation.

ACKNOWLEDGMENT

On the occasion of my 65th birthday and of the ensuing mandatory retirement from CEA-Saclay, I express my deepest gratitude to all the individuals, colleagues, and friends who have helped me, through collaborations, discussions, or even healthy competition, to develop and apply the technique of FTIR difference spectroscopy to the field of photosynthetic reactions.

SUPPORTING INFORMATION AVAILABLE

ASCII file of the spectrum displayed in Figure 4A. This material is available free of charge via the Internet at http://pubs.acs.org.

REFERENCES

1. Okamura, M. Y., Paddock, M. L., Graige, M. S., and Feher, G. (2000) Proton and electron transfer in bacterial reaction centers, *Biochim. Biophys. Acta 1458*, 148−163.
2. Wraight, C. A. (2004) Proton and electron transfer in the acceptor quinone complex of photosynthetic reaction centers from *Rhodobacter sphaeroides*, *Front. Biosci. 9*, 309−337.
3. Tiede, D. M., Utschig, L., Hanson, D. K., and Gallo, D. M. (1998) Resolution of electron and proton transfer events in the electrochromism associated with quinone reduction in bacterial reaction centers, *Photosynth. Res. 55*, 267−273.
4. Graige, M. S., Feher, G., and Okamura, M. Y. (1998) Conformational gating of the electron transfer reaction $Q_A^{-\bullet}Q_B \rightarrow Q_AQ_B^{-\bullet}$ in bacterial reaction centers of *Rhodobacter sphaeroides* determined by a driving force assay, *Proc. Natl. Acad. Sci. U.S.A. 95*, 11679−11684.
5. Li, J., Takahashi, E., and Gunner, M. R. (2000) $-\Delta G°_{AB}$ and pH dependence of the electron transfer from $P^+Q_A^-Q_B$ to $P^+Q_AQ_B^-$ in *Rhodobacter sphaeroides* reaction centers, *Biochemistry 39*, 7445−7454.
6. Li, J., Gilroy, D., Tiede, D. M., and Gunner, M. R. (1998) Kinetic phases in the electron transfer from $P^+Q_A^-Q_B$ to $P^+Q_AQ_B^-$ and the associated processes in *Rhodobacter sphaeroides* R-26 reaction centers, *Biochemistry 37*, 2818−2829.
7. Stowell, M. H. B., McPhillips, T. M., Rees, D. C., Soltis, S. M., Abresch, E., and Feher, G. (1997) Light-induced structural changes in photosynthetic reaction center: Implications for mechanism of electron-proton transfer, *Science 276*, 812−816.
8. Xu, Q., Baciou, L., Sebban, P., and Gunner, M. R. (2002) Exploring the energy landscape for Q_A^- to Q_B electron transfer in bacterial photosynthetic reaction centers: Effect of substrate position and tail length on the conformational gating step, *Biochemistry 41*, 10021−10025.
9. Breton, J., Boullais, C., Mioskowski, C., Sebban, P., Baciou, L., and Nabedryk, E. (2002) Vibrational spectroscopy favors a unique Q_B binding site at the proximal position in wild-type reaction centers and in the Pro-L209 → Tyr mutant from *Rhodobacter sphaeroides*, *Biochemistry 41*, 12921−12927.
10. Nabedryk, E., Breton, J., Sebban, P., and Baciou, L. (2003) Quinone (Q_B) binding site and protein structural changes in photosynthetic reaction centers mutants at Pro-L209 revealed by vibrational spectroscopy, *Biochemistry 42*, 5819−5827.
11. Breton, J. (2004) Absence of large-scale displacement of quinone Q_B in bacterial photosynthetic reaction centers, *Biochemistry 43*, 3318−3326.
12. Baxter, R. H. G., Ponomarenko, N., Srajer, V., Pahl, R., Moffat, K., and Norris, J. R. (2004) Time-resolved crystallographic studies of light-induced structural changes in the photosynthetic reaction center, *Proc. Natl. Acad. Sci. U.S.A. 101*, 5982−5987.
13. Potter, J. A., Fyfe, P. K., Frolov, D., Wakeham, M. C., van Grondelle, R., Robert, B., and Jones, M. R. (2005) Strong effects of an individual water molecule on the rate of primary charge separation in the *Rhodobacter sphaeroides* reaction centre, *J. Biol. Chem. 280*, 27155−27164.
14. Debus, R. J., Feher, G., and Okamura, M. Y. (1986) Iron-depleted reaction centers from *Rhodopseudomonas sphaeroides* R-26.1: Characterization and reconstitution with Fe^{2+}, Mn^{2+}, Co^{2+}, Ni^{2+}, Cu^{2+} and Zn^{2+}, *Biochemistry 25*, 2276−2287.
15. Feher, G., and Okamura, M. Y. (1999) The primary and secondary acceptors in bacterial photosynthesis: II. The structure of the Fe^{2+}-$Q^{\bullet-}$ complex, *Appl. Magn. Reson. 16*, 63−100.
16. Lubitz, W., and Feher, G. (1999) The primary and secondary acceptors in bacterial photosynthesis: III. Characterization of the quinone radicals by EPR and ENDOR, *Appl. Magn. Reson. 17*, 1−48.
17. Thibodeau, D. L., Nabedryk, E., Hienerwadel, R., Lenz, F., Mäntele, W., and Breton, J. (1990) Time-resolved FTIR spectroscopy of quinones in *Rb. sphaeroides* reaction centers, *Biochim. Biophys. Acta 1020*, 253−259.
18. Mäntele, W., Leonhard, M., Bauscher, M., Nabedryk, E., Breton, J., and Moss, D. A. (1990) in *Reaction Centers of Photosynthetic Bacteria* (Michel-Beyerle, M.-E., Ed.) pp 31−44, Springer-Verlag, Berlin.
19. Breton, J., Thibodeau, D. L., Berthomieu, C., Mäntele, W., Verméglio, A., and Nabedryk, E. (1991) Probing the primary quinone (Q_A) environment in photosynthetic bacterial reaction centers by light-induced FTIR difference spectroscopy, *FEBS Lett. 278*, 257−260.
20. Breton, J., Berthomieu, C., Thibodeau, D. L., and Nabedryk, E. (1991) Probing the secondary quinone (Q_B) environment in photosynthetic bacterial reaction centers by light-induced FTIR difference spectroscopy, *FEBS Lett. 288*, 109−113.
21. Breton, J., Burie, J.-R., Berthomieu, C., Berger, G., and Nabedryk, E. (1994) The binding-sites of quinones in photosynthetic bacterial reaction centers investigated by light-induced FTIR difference spectroscopy: Assignment of the Q_A vibrations in *Rhodobacter sphaeroides* using ^{18}O- or ^{13}C-labeled ubiquinone and vitamin K_1, *Biochemistry 33*, 4953−4965.
22. Breton, J., Boullais, C., Burie, J.-R., Nabedryk, E., and Mioskowski, C. (1994) Binding-sites of quinones in photosynthetic bacterial reaction centers investigated by light-induced FTIR difference spectroscopy: Assignment of the interactions of each carbonyl of Q_A in *Rhodobacter sphaeroides* using site-specific ^{13}C-labeled ubiquinone, *Biochemistry 33*, 14378−14386.
23. Brudler, R., de Groot, H. J. M., van Liemt, W. B. S., Steggerda, W. F., Esmeijer, R., Gast, P., Hoff, A. J., Lugtenburg, J., and Gerwert, K. (1994) Asymmetric binding of the 1- and 4-C═O groups of Q_A in *Rhodobacter sphaeroides* R26 reaction centers monitored by Fourier transform infra-red spectroscopy using site-specific isotopically labelled ubiquinone-10, *EMBO J. 13*, 5523−5530.
24. Breton, J., Boullais, C., Berger, G., Mioskowski, C., and Nabedryk, E. (1995) Binding-sites of quinones in photosynthetic bacterial reaction centers investigated by light-induced FTIR difference spectroscopy: Symmetry of the carbonyl interactions and close equivalence of the Q_B vibrations in *Rhodobacter sphaeroides* and *Rhodopseudomonas viridis* probed by isotope labeling, *Biochemistry 34*, 11606−11616.
25. Brudler, R., de Groot, H. J. M., van Liemt, W. B. S., Gast, P., Hoff, A. J., Lugtenburg, J., and Gerwert, K. (1995) FTIR spectroscopy shows weak symmetric hydrogen bonding of the Q_B carbonyl groups in *Rhodobacter sphaeroides* R26 reaction centers, *FEBS Lett. 370*, 88−92.
26. Breton, J., and Nabedryk, E. (1996) Protein-quinone interactions in the bacterial photosynthetic reaction center: Light-induced FTIR difference spectroscopy of the quinone vibrations, *Biochim. Biophys. Acta 1275*, 84−90.
27. Hienerwadel, R., Grzybek, S., Fogel, C., Kreutz, W., Okamura, M. Y., Paddock, M. L., Breton, J., Nabedryk, E., and Mäntele, W. (1995) Protonation of Glu L212 following Q_B^- formation in the photosynthetic reaction center of *Rhodobacter sphaeroides*: Evidence from time-resolved infrared spectroscopy, *Biochemistry 34*, 2832−2843.
28. Brudler, R., and Gerwert, K. (1998) Step-scan FTIR spectroscopy resolves the $Q_A^-Q_B \rightarrow Q_AQ_B^-$ transition in *Rb. sphaeroides* R26 reaction centres, *Photosynth. Res. 55*, 261−266.
29. Remy, A., and Gerwert, K. (2003) Coupling of light-induced electron transfer to proton uptake in photosynthesis, *Nat. Struct. Biol. 10*, 637−644.
30. Butler, W. F., Johnston, D. C., Shore, H. B., Fredkin, D. R., Okamura, M. Y., and Feher, G. (1980) The electronic structure of Fe^{2+} in reaction centers from *Rhodopseudomonas sphaeroides*. I. Static magnetization measurements, *Biophys. J. 32*, 967−992.

31. Eisenberger, P., Okamura, M. Y., and Feher, G. (1982) The electronic structure of Fe^{2+} in reaction centers from *Rhodopseudomonas sphaeroides*. II. Extended X-ray fine structure study, *Biophys. J. 32*, 523−538.
32. Hermes, S., Bremm, O., Garczarek, F., Derrien, V., Liebisch, P., Loja, P., Sebban, P., Gerwert, K., and Haumann, M. (2006) A time-resolved iron-specific X-ray absorption experiment yields no evidence for an $Fe^{2+} \rightarrow Fe^{3+}$ transition during $Q_A \rightarrow Q_B$ electron transfer in the photosynthetic reaction center, *Biochemistry 45*, 353−359.
33. Hermes, S., Stachnik, J. M., Onidas, D., Remy, A., Hofmann, E., and Gerwert, K. (2006) Proton uptake in the reaction center mutant L210DN from *Rhodobacter sphaeroides* via protonated water molecules, *Biochemistry 45*, 13741−13749.
34. Nabedryk, E., Breton, J., Hienerwadel, R., Fogel, C., Mäntele, W., Paddock, M. L., and Okamura, M. Y. (1995) Fourier transform infrared difference spectroscopy of secondary quinone acceptor photoreduction in proton transfer mutants of *Rhodobacter sphaeroides*, *Biochemistry 34*, 14722−14732.
35. Nabedryk, E., Breton, J., Okamura, M. Y., and Paddock, M. L. (2001) Simultaneous replacement of Asp-L210 and Asp-M17 with Asn increases proton uptake by Glu-L212 upon first electron transfer to Q_B in reaction centers from *Rhodobacter sphaeroides*, *Biochemistry 40*, 13826−13832.
36. Mezzetti, A., Nabedryk, E., Breton, J., Okamura, M. Y., Paddock, M. L., Giacometti, G., and Leibl, W. (2002) Rapid-scan Fourier transform infrared spectroscopy shows coupling of Glu-L212 protonation and electron transfer to Q_B in *Rhodobacter sphaeroides* reaction centers, *Biochim. Biophys. Acta 1553*, 320−330.
37. Jones, L. H. (1963) Nature of bonding in metal cyanide complexes as related to intensity and frequency of infrared absorption spectra, *Inorg. Chem. 2*, 777−780.
38. Breton, J., and Nabedryk, E. (1998) Proton uptake upon quinone reduction in bacterial reaction centers: IR signature and possible participation of a highly polarizable hydrogen bond network, *Photosynth. Res. 55*, 301−307.
39. Breton, J., Bibikova, M., Oesterhelt, D., and Nabedryk, E. (1998) Electrostatic influence of Q_A or Q_B reduction on the 10a-ester vibration of H_A in *Rps. viridis*, in *Photosynthesis: Mechanisms and Effects* (Garab, G., Ed.) Vol. 2, pp 687−692, Kluwer Academic Publishers, Dordrecht, The Netherlands.
40. Miksovska, J., Schiffer, M., Hanson, D. K., and Sebban, P. (1999) Proton uptake by bacterial reaction centers: The protein complex responds in a similar manner to the reduction of either quinone acceptor, *Proc. Natl. Acad. Sci. U.S.A. 96*, 14348−14353.
41. Breton, J., Richaud, P., Verméglio, A., and Nabedryk, E. (2001) Infrared vibrational modes of histidine ligands of the primary electron donor and of Q_A in purple photosynthetic bacteria, *PS2001 Proceedings of the 12th International Congress on Photosynthesis*, S7-002, CSIRO Publishing, Collingwood, Victoria, Australia.
42. Brzezinski, P., Okamura, M. Y., and Feher, G. (1992) Structural changes following the formation of $D^+Q_A^-$ in bacterial reaction centers: Measurement of light-induced electrogenic events in RCs incorporated in a phospholipid monolayer, in *The Photosynthetic Bacterial Reaction Center II* (Breton, J., and Verméglio, A., Eds) pp 321−330, Plenum Press, New York.

BI700297B